FESOM2.1-REcoM3-MEDUSA2: an ocean-sea ice-biogeochemistry model coupled to a sediment model

Ying Ye[1], Guy Munhoven[2], Peter Köhler[1], Martin Butzin[1,3], Judith Hauck[1], Özgür Gürses[1], and Christoph Völker[1]

[1]Alfred-Wegener-Institut Helmholtz-Zentrum für Polar- und Meeresforschung (AWI), P.O. Box 12 01 61, 27515 Bremerhaven, Germany
[2]Laboratoire de Physique Atmosphérique et Planétaire, Université de Liège, B–4000 Liège, Belgium
[3]MARUM — Center for Marine Environmental Sciences, University of Bremen, Bremen, Germany

Correspondence: Ying Ye (Ying.Ye@awi.de)

Abstract.

This study describes the coupling of the process-based Model of Early Diagenesis in the Upper Sediment (MEDUSA version 2) to an existing ocean biogeochemistry model consisting of the Finite-volumE Sea ice-Ocean Model (FESOM version 2.1) and the Regulated Ecosystem Model (REcoM version 3). Atmospheric CO_2 in the model is a prognostic variable which is determined by the carbonate chemistry in the surface ocean. The model setup and its application to a pre-industrial control climate state is described in detail. In the coupled model 400 PgC are stored in equilibrium in the top 10 cm of the bioturbated sediment, mainly as calcite, but also to 5% as organic matter. Simulated atmospheric CO_2 is in equilibrium at 286 ppm in the coupled simulation, which is close to the initially assumed value of the pre-industrial CO_2 level. Sediment burial of carbon, alkalinity and nutrients in the coupled simulation is set to be partly compensated by riverine input. The spatial distribution of biological production is altered depending on the location of riverine input and the strength of local nutrient limitation, while the global productivity is not affected substantially.

1 Introduction

The ocean plays a key role in the global carbon cycle. It stores about 37,200 PgC (Keppler et al., 2020), more than 40 times as much carbon as the atmosphere, which contained 884 PgC (or 417 ppm) in the year 2022 (Lan et al., 2023). About 25–30% of the global anthropogenic CO_2 emissions are taken up by the world oceans (Friedlingstein et al., 2022).

CO_2 enters the ocean through gas-exchange, where it dissolves in seawater. A unique feature of dissolved CO_2 is that it reacts with water to form carbonic acid, which is instable and dissociates into bicarbonate, carbonate and hydrogen ions. The dissolved inorganic carbon (DIC), which is the sum of CO_2, bicarbonate ion HCO_3^- and carbonate ion CO_3^{2-}, is distributed in the ocean via circulation. Part of the carbon in the surface ocean is also taken up via photosynthesis by marine phytoplankton and exported into the ocean interior via the sinking of dead organic matter. When stored in the deep ocean, this carbon reduces the surface concentration of DIC and allows for further CO_2 uptake from the atmosphere. Another important process in the marine carbon cycle is driven by calcifying plankton. They produce calcium carbonate ($CaCO_3$) shells whereby CO_2 is released

back into the atmosphere. These processes which all influence the surface-to-depth-gradient in DIC are also summarized as the so-called marine carbon pumps (Volk and Hoffert, 1985). Some of the particulate carbon (i.e. particulate organic carbon and $CaCO_3$, ca. 1% of primary production; Sarmiento and Gruber, 2006) escapes dissolution and remineralization in the water column and sinks to the seafloor, where it might be buried. These particles are then subtracted from the relatively fast cycling of carbon at the surface of the Earth.

The storage of carbon, alkalinity and nutrients in sediments adds an additional slow timescale to carbon cycling, and overall increases the carbon storage in the sediment-ocean system. The sinking flux of particulate organic carbon (POC) to the surface sediment is commonly reported to be within the range of 120–210 $PgC\,kyr^{-1}$ (Berner, 1989; Hedges and Keil, 1995; Sarmiento and Gruber, 2006), although there are significantly higher estimates in the literature as well, e.g. 310 $PgC\,kyr^{-1}$ by Burdige (2007) or 340 $PgC\,kyr^{-1}$ by Sarmiento et al. (2002). The sinking flux of $CaCO_3$ is estimated to lie between 100–150 $PgC\,kyr^{-1}$ (Catubig et al., 1998; Sarmiento and Gruber, 2006; Dunne et al., 2012) in deep waters. In shallow waters these fluxes are even higher (Cartapanis et al., 2018). Furthermore, marine sediments play an important role in recording the Earth's past climate and react via the carbonate compensation feedback to any changes in the marine carbon cycle, in which the deep ocean carbonate ion concentration is brought back to its initial values after a perturbation on a multi-millennial timescale via sediment dissolution of $CaCO_3$ (Broecker and Peng, 1987).

Anthropogenic carbon emissions represent an extreme carbon cycle perturbation and will ultimately lead to the massive dissolution of $CaCO_3$ in seafloor sediments over the next millennia (Archer et al., 1997). This carbonate compensation feedback contributes to a reduction of the long-term airborne fraction of anthropogenically emitted CO_2 from more than 20% if only the atmosphere-ocean is considered to be less than 10% (Archer et al., 2009; Köhler, 2020). This additional oceanic uptake of anthropogenic carbon through the dissolution of $CaCO_3$, however, operates on a timescale longer than 10,000 yr, and is therefore only of interest for the geological fate of fossil emissions, but not for our near future.

Hence, understanding processes controlling the sediment-ocean exchange and quantifying the carbon storage in marine sediments are crucial to explain transient behaviour over changing climates, e.g. the glacial-interglacial CO_2 variations (e.g. Brovkin et al., 2012; Köhler and Munhoven, 2020), and to predict the long-term ocean sequestration of anthropogenic carbon (Archer et al., 2009; Köhler, 2020).

All ocean biogeochemistry models incorporate a scheme to describe the fate of biogenic material that reaches the seafloor, but differ in their complexity (Munhoven (2021) and references therein). The most simple schemes start from a reflective boundary condition, where all material reaching the seafloor is remineralized and returned to solution. More complex scheme consider a single, vertically integrated mixed-layer sediment box with a complete mass balances for the particles settling to the seafloor. And higher complexity is found in vertically resolved sediment models describing diagenetic reactions, mechanical changes of dissolved and solid components as well as burial fluxes out of the surface sediment.

FESOM2.1-REcoM3, consisting of the Finite-volumE Sea ice-Ocean Model 2.1 and the Regulated Ecosystem Model 3, is one of the ocean biogeochemistry models which so far includes a simple one-layer sediment model (Gürses et al., 2023). REcoM3 describes the marine ecosystem at medium complexity with two phytoplankton classes including silicifiers and calcifiers, two zooplankton classes representing copepods and krill, and considers flexible stoichiometry of C, N, Si, Fe, $CaCO_3$,

and chlorophyll. Various iron sources (sediment, dust and rivers) are implemented into REcoM3 and the model also has the option to simulate the cycles of ^{13}C and ^{14}C (Butzin et al., 2023). The sediment box used so far in REcoM3 ensures the mass

60   conservation by a complete remineralization of material sinking into the box. It represents processes in the surface sediment and is useful for short-term simulations, since remineralization happens within hours and days, while sedimentation and weathering have time scale of thousands of years. Kriest and Oschlies (2013) have shown that the introduction of a sediment box makes models more robust against the uncertainties of the remineralization length scale, compared to models that remineralize everything in the water column. However, without considering sediment-ocean fluxes and feedbacks in more detail the model

65   would not be able to reasonably simulate transient changes over glacial/interglacial timescales.

In this study, we describe (Section 2) the coupling of FESOM2.1-REcoM3 with the Model of Early Diagenesis in the Upper Sediment (MEDUSA2) (Munhoven, 2021), a complex process-based sediment module that offers an alternative to the previously used one-layer sediment. Using a configuration of FESOM2.1-REcoM3 targeted for paleoclimate research, referred to as FESOM2.1-REcoM3p, we performed a coupled ocean-sediment simulation under pre-industrial climate conditions and

70   present results of sediment distribution and carbon storage of this simulation in Section 3.

2   Methods

2.1   Model description

2.1.1   A REcoM3 configuration for paleo research – REcoM3p

REcoM is an ocean biogeochemistry and ecosystem model describing cycles of carbon, oxygen and nutrients (nitrogen, silicon

75   and iron) with varying intracellular stoichiometry in phytoplankton, zooplankton and detritus. REcoM3 is the most recent release version and a detailed description of this version including its coupling to FESOM2.1 is given by Gürses et al. (2023). In this study we used a configuration with reduced complexity of REcoM3 mainly with respect to functional groups of the modelled ecosystem and considered only one generic zooplankton and one detritus class, instead of two in the full version of REcoM3 (Fig. 1). Like in the full version, diatoms and small phytoplankton which implicitly include calcifiers (only calcite

80   producers, no aragonite) are considered here. REcoM3 was extended, on the other hand, comparing to the version described by Gürses et al. (2023) for application in paleoclimate research. A riverine source of dissolved iron (DFe) was added to the already existing two sources from dust and marine sediments. Due to the coupling to MEDUSA2, the sedimentary source of iron can be calculated in two ways: 1) in a fixed ratio to degradation of particulate organic nitrogen (PON) in the benthic layer as described in Gürses et al. (2023, Eq. A77 in Appendix A) or 2) in a fixed ratio to the diffusive flux of dissolved

85   inorganic nitrogen (DIN) calculated by MEDUSA2 in coupled simulations. The same Fe:N ratio is used for both methods. A comparison of source strengths for iron is shown in Section 3.3. Furthermore, carbon isotopes were implemented into REcoM3, as described in Butzin et al. (2023). The coupling with MEDUSA2 regarding carbon isotopes is currently under development. Here, we describe the coupling of the modified REcoM3 configuration (REcoM3p with carbon isotopes switched off) with the sediment model MEDUSA2.
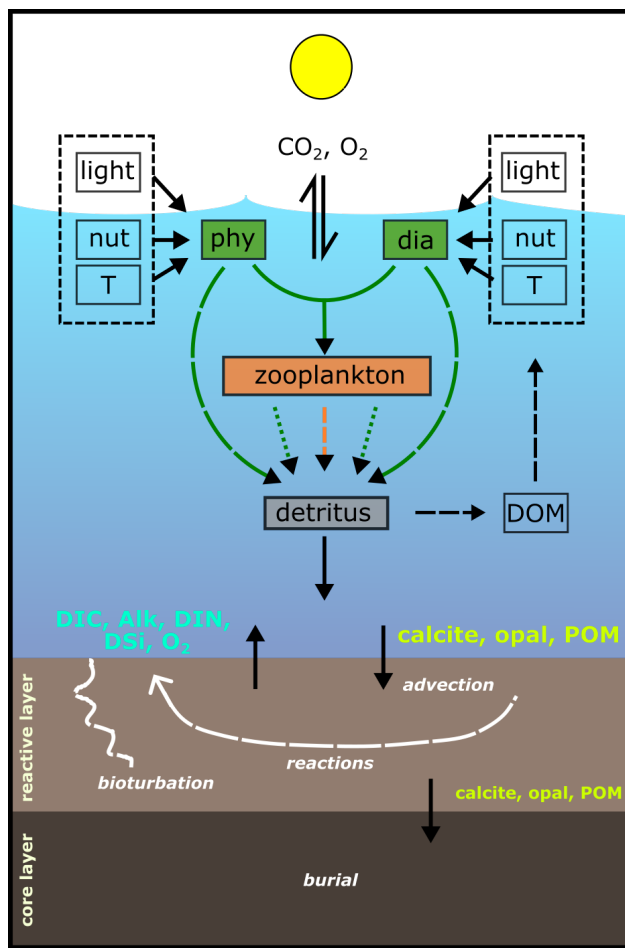
Figure 1. Schematic diagram of the components and interactions in REcoM3p coupled with the sediment model MEDUSA2 (modified and extended from Gürses et al. (2023, Fig. 2)). Small phytoplankton (**phy**) and diatoms (**dia**) take up inorganic nutrients (**nut**) and grow in dependence on **light** and temperature (**T**). One generic **zooplankton** consumes phytoplankton. Phytoplankton aggregation, zooplankton sloppy feeding, mortality and fecal pellets generate sinking **detritus**. Sinking detritus degrades to dissolved organic matter (**DOM**) which then remineralizes to dissolved inorganic carbon (DIC) and nitrogen (DIN). **Calcite**, **opal** and particulate organic matter (**POM**) reaching the seafloor enter the reactive layer of sediments, where accumulation, bioturbation, degradation and dissolution take place. Dissolved products of these processes (**DIC, DIN, Alk, DSi, and** O_2) go back to the bottom water by diffusion. The solids accumulate and are buried further in the core layer.

2.1.2 The sediment model MEDUSA2

MEDUSA is a time-dependent one-dimensional numerical model of coupled early diagenetic processes in sea-floor surface sediments. The original model version was described in Munhoven (2007), but that version has been further developed to MEDUSA2 which allows for a flexible chemical composition of the sediment, of the chemical transformations that describe

the diagenetic processes (e.g. denitrification), and chemical equilibria to consider, and also offers a variety of Application Pro-
95 gramming Interfaces (APIs) for coupling it to ocean models with different grid configurations and biogeochemical components
(Munhoven, 2021).

In MEDUSA a sediment column is divided into two main realms. The topmost part from the sediment surface is the 'reactive'
layer where solids sinking from the bottom layer of the ocean are collected. Here, chemical reactions take place, solids are
transported by bioturbation and advection resulting from the continuous deposition of new material, and solutes by molecular
100 diffusion and bioirrigation. The second realm is the layer underneath the reactive layer, also called core layer. Here, no reactions
or mixing take place. Solids are buried and preserved in this layer which is building up a synthetic sediment core. In our
coupled configuration MEDUSA2 sediment columns (one per seafloor grid element) only resolve a 10 cm thick reactive
surface sediment layer on a vertical grid with 21 points. The grid point spacing is not regular but increases with depth in the
sediment in order to allow for a better representation of the strong subsurface solute concentration gradients. The burial flux
105 from the reactive layer into the core layer were monitored in our simulations, but not the changes of solids in the core layer.
Only exchange between a single sediment column and its overlying ocean grid cell was considered in the coupling, i.e. there is
no lateral exchange between sediment columns.

MEDUSA has already been coupled to several ocean biogeochemistry and Earth System Models (Moreira Martinez et al.,
2016; Kurahashi-Nakamura et al., 2020; Munhoven, 2021). Coupling to ocean models is done through so-called 'applications'
110 in the MEDUSA code. We introduced a new application "medusa-fesom-recom" which regulates 1) the reading of FESOM2.1-
REcoM3p input and conversion into format and units that MEDUSA needs, 2) selecting of processes and global rate parameter
values for tracing the evolution of the concentrations of solids and solutes considered, and 3) writing the resulting diffusive
solute exchange with the ocean to a file for usage by FESOM2.1-REcoM3p and the obtained burial loss of solids into the
sediment core. These burial losses can be used to monitor and/or regulate oceanic mass balances for the main nutrients (nitrogen
115 and silicon), and alkalinity.

Consistent with the input from FESOM2.1-REcoM3p, we chose a MEDUSA2 configuration with five solids (clay, calcite,
opal and two types of organic matter) and six solute components (CO_2, HCO_3^-, CO_3^{2-}, O_2, NO_3^- and H_4SiO_4). The two
types of organic matter are needed to account for the variable stoichiometry in REcoM3p. Processes altering the content of
solids and solutes in sediments include calcite dissolution, oxic respiration of organic matter, organic matter degradation by
120 denitrification, opal dissolution, chemical equilibria of the carbonate system and burial. REcoM3p only calculates formation
and dissolution of calcite and does not represent aragonite. Correspondingly, only calcite dissolution in sediments is considered
in the MEDUSA2 application "medusa-fesom-recom".

Biological components in REcoM3p have variable intracellular stoichiometry and thus the sinking fluxes of POC and PON
(particulate organic nitrogen) have no fixed ratio. However, in MEDUSA2 degradation of particulate organic matters (POM) is
125 calculated for POM classes with a fixed stoichiometry. We therefore defined two end-member POM classes in MEDUSA2 in
which $Q = C : N$ is fixed with $Q_1 = 106 : 21$ and $Q_2 = 200 : 11$, respectively, representing the minimum and maximum C:N
ratio simulated in the sinking flux in REcoM3p. The total outgoing fluxes of PON from REcoM3p (F_N^o) were than partitioned

into two incoming contributions F_N^{i1} and F_N^{i2}, according to

$$F_N^{i1} = \frac{Q_2 - Q}{Q_2 - Q_1} \cdot F_N^{o} \tag{1}$$

$$F_N^{i2} = \frac{Q - Q_1}{Q_2 - Q_1} \cdot F_N^{o} \tag{2}$$

where $Q = F_C^o / F_N^o$ is the ratio of the POC flux (F_C^o) to the PON flux (F_N^o) that reaches the seafloor in REcoM3p. The carbon fluxes carried by the two POM classes are finally calculated by multiplying F_N^{i1} and F_N^{i2} nitrogen fluxes with the respective C:N ratios:

$$F_C^{i1} = Q_1 \cdot F_N^{i1} \tag{3}$$

$$F_C^{i2} = Q_2 \cdot F_N^{i2} \tag{4}$$

Besides organic matter, calcite and opal, the simulated sediment contains an inert component, which we refer to as 'clay' here for the sake of simplicity, and which is ultimately delivered from land. It stems from dust particles deposited over the sea surface and from terrestrial materials transported to the oceans by rivers. In our model setup, annual mean dust deposition from Albani et al. (2014) is considered as the oceanic clay input into sediments. Further, a globally constant input of $2.5 \cdot 10^{-8}$ mol illite cm^{-2} year^{-1} over the seafloor is added to mimic the terrestrial component in clay following Heinze et al. (1999), assuming that clay has the composition of illite.

2.2 Coupling REcoM3p and MEDUSA2

FESOM2.1-REcoM3p and MEDUSA2 are sequentially coupled through file exchange. Sinking fluxes of POC, PON, opal (SiO$_2$) and calcite out of the bottom water boxes are saved as output files by FESOM2.1-REcoM3p and read as input files by MEDUSA2 (Fig. 1). Furthermore, MEDUSA2 requires information on temperature, salinity and concentrations of alkalinity (Alk), DIC, oxygen, and nutrients in the bottom-most ocean model box. Temperature and salinity enter thermodynamic calculations in the sediment model and the bottom water concentrations into the calculation of diffusive fluxes between sediment and water column.

FESOM2.1-REcoM3p reads diffusive fluxes of nutrients including dissolved inorganic nitrogen (DIN) and dissolved silicate (DSi or H$_4$SiO$_4$), DIC, Alk and oxygen from MEDUSA2 output file (Fig. 1). DFe input from sediments is derived from the diffusive flux of DIN, using a fixed Fe:N ratio. Another output of MEDUSA2 is the permanent burial of carbon, organic matter, opal and calcite in the sediment core. This output is used to monitor, and partly compensate, changes in the total mass balances of the ocean and reactive sediment. For silicon and nitrogen we assumed that riverine input compensates the burial flux, while for Alk, a global riverine input was taken from Börker et al. (2020) representing weathering fluxes. Based on the sediment burial of carbon (POC and calcite, Table 2), we slightly tuned DIC river input to reproduce the pre-industrial CO$_2$ level. The total riverine input is distributed over the surface ocean in the model by scaling it with the local river runoff from the forcing data.

2.3 Model setup

2.3.1 Model configuration

160 FESOM2.1 employs unstructured meshes with variable horizontal resolution. The default mesh of FESOM2.1-REcoM3 (COR-EII mesh) has about 127000 surface nodes with a nominal average resolution of 1 degree and enhanced resolution in the equatorial belt and in high latitudes going up to 25 km (Gürses et al., 2023). For testing the coupling with MEDUSA2 a reduced model resolution (PI mesh) is used here, containing 3140 surface nodes, corresponding to a median horizontal resolution of 260 km (Butzin et al., 2023). This configuration reduces computational costs and simplifies simulations over the time scale of

165 thousands of years in order to approach deep ocean equilibrium and significant changes in marine sediments. Vertically, the ocean is divided into 47 layers and the layer thickness ranges from 5 m in the surface to 250 m in the deep ocean. The full free-surface formulation (zstar) was used, allowing vertical movement of all layers, to ensure tracer conservation in FESOM (Scholz et al., 2019, 2022). In this study, the model was retuned for the coarser resolution by reducing the maximum thickness diffusivity of the Gent-McWilliams parameterisation from 3000 m^2 s^{-1} (used in the default FESOM2.1) to 1000 m^2 s^{-1}.

170 REcoM3p configured for this study includes 22 biogeochemical tracers, covering nutrients (DIN, DSi and DFe), two types of phytoplankton (diatoms and small phytoplankton) with the state variables C, N and chlorophyll, as well as biogenic silica in diatoms and calcite in small phytoplankton, one zooplankton with C and N pools, one detritus with the state variables C, N, calcite and opal, dissolved organic matter with C and N pools, DIC, Alk and oxygen. Because of a reduced foodweb compared to REcoM3, parameter values for REcoM3p were taken from a previous REcoM version (REcoM2) coupled to FESOM1.4

175 (Schourup-Kristensen et al., 2014). MEDUSA2 is coupled to the bottom layers of the ocean model, therefore the horizontal grid within MEDUSA2 is always the same as in the ocean model.

Atmospheric CO_2 concentrations are calculated assuming that the atmosphere can be represented as an instantaneously mixed carbon reservoir, and disregarding the carbon cycle on land. Temporal changes in the atmospheric volume mixing ratio of CO_2 (X_{CO_2} in ppm) then correspond to the globally integrated CO_2 air-sea gas exchange flux, i.e.

180
$$\frac{\delta X_{CO_2}}{\delta t} = -\frac{\rho_{air}}{m_{atm}} \cdot 10^6 \int F_{CO_2} \, dA \tag{5}$$

where F_{CO_2} (mol m^{-2} s^{-1}) is the regional air-sea CO_2 gas flux (calculated according to Wanninkhof (2014)), dA integrates over the ocean area, $\rho_{air} = 0.02897$ kg mol^{-1} is the mean density of dry air (Williams, 2023), and $m_{atm} = 5.1352 \cdot 10^{18}$ kg is the mass of the dry atmosphere (Trenberth and Smith, 2005). The factor 10^6 serves to convert from mol mol^{-1} to ppm. In this study, the initial value of X_{CO_2} is 284.3 ppm following Meinshausen et al. (2017).

2.3.2 Forcing and initial conditions

185

FESOM2.1 is initialised with seasonal winter temperatures and salinities from the Polar Science Center Hydrographic Climatology (PHC3, updated from Steele et al. (2001)) and driven by annually repeated atmospheric fields using the Corrected Normal Year Forcing Version 2.0 (CORE-NYF.v2, Large and Yeager, 2009).
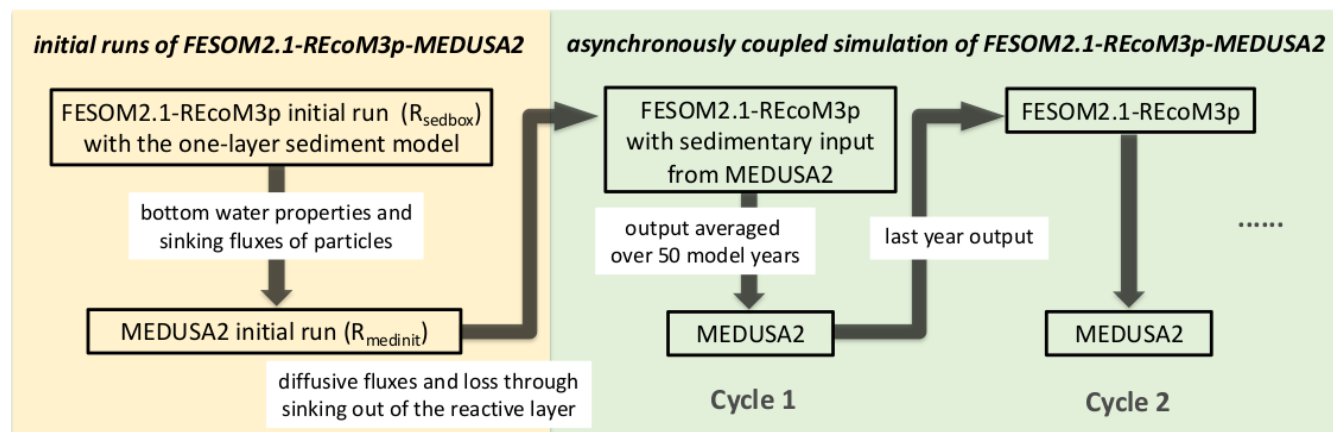
Figure 2. Workflow of a coupled FESOM2.1-REcoM3p-MEDUSA2 simulation.

Alk and DIC are initialised from version 2 of the Global Ocean Data Analysis Project (GLODAPv2) data set (Lauvset et al., 2016), DIN and DSi from the Levitus World Ocean Atlas climatology of 2013 (Garcia et al., 2014) and oxygen from the Levitus World Ocean Atlas climatology of 2018 (Garcia et al., 2019). The initial DFe field stems from the Pelagic Interaction Scheme for Carbon and Ecosystem Studies (PISCES) model (Aumont et al., 2015).

Dust input of iron at the sea surface is calculated based on monthly averages of dust deposition by Albani et al. (2014) with a weight percentage for iron of 3.5% and a solubility of 2%. Total riverine input of DFe is assumed to be $2.6 \cdot 10^9 \, \mathrm{mol \, Fe \, year^{-1}}$ (de Baar and de Jong, 2001). It is distributed at the sea surface by scaling with the river runoff, which is part of the CORE-NYF.v2 forcing.

2.4 Coupled simulation with FESOM2.1-REcoM3p-MEDUSA2

A coupled simulation starts with an initial FESOM2.1-REcoM3p run, followed by an initial MEDUSA2 run. Subsequently, FESOM2.1-REcoM3p and MEDUSA2 are run alternately with a defined coupling frequency of 50 years (Fig. 2).

2.4.1 Initial FESOM2.1-REcoM3p run ($\mathbf{R_{sedbox}}$)

FESOM2.1 was run for 1000 years as a spinup of the ocean circulation. After that, REcoM3p was switched on and run for another 1000 years to get a quasi-equilibrium of deep ocean concentrations. During these 1000 years, the exchange between ocean and sediment was calculated with the one-box sediment that was already integrated in REcoM3p. Model output of the last 50 years was analysed as the initial FESOM2.1-REcoM3p run ($\mathrm{R_{sedbox}}$).

2.4.2 Initial MEDUSA2 run ($\mathbf{R_{medinit}}$)

Continuous exchange with sediments alters both ocean boundary conditions and properties of sediments. The latter changes much more slowly due to low sedimentation rates. To reduce the computing time for getting significant changes in sediments,

MEDUSA2 was first run for 100,000 years driven by input from R_{sedbox} so that the sediment layers in MEDUSA are filled up before an interactive coupled FESOM2.1-REcoM3p-MEDUSA2 simulation starts.

2.4.3 Coupled simulation ($R_{coupled}$)

Two simulations were conducted in this study to demonstrate how carbon storage in sediments affects the marine carbon cycle and atmospheric CO_2 (Fig. 2): (1) We continued the R_{sedbox} simulation without MEDUSA2 but the one-layer sediment for 2500 model years after initialization; (2) a coupled simulation $R_{coupled}$ was conducted for 1500 model years first using the output from $R_{medinit}$ as sedimentary input of DIC, Alk and nutrients. A coupling frequency of 50 years was consistently applied for FESOM2.1-REcoM3p and MEDUSA2. For each coupling cycle, output of FESOM2.1-REcoM3p was averaged over 50 years and used to drive MEDUSA2. And the sedimentary input for FESOM2.1-REcoM3p was updated every 50 years with results from the MEDUSA2 simulation. The same ocean-sediment exchange fluxes were applied at each time step within one coupling cycle. Outputs of R_{sedbox} and $R_{coupled}$ were averaged over the last 50 years for analysis.

2.4.4 Performance of coupled simulation

FESOM coupled with REcoM spends about 80% of the total run time of a simulation on the tracer transport computations (Himstedt, 2023). An acceleration method was implemented for a parallel calculation of tracer advection and with two parallel tracer groups on 72 cores, a good relative speedup of 1.8 was achieved for simulations in the PI mesh (Himstedt, 2023). In this study, a coupled FESOM2.1-REcoM3-MEDUSA2 cycle (50 model years) is then completed within seven hours computation time with 72 cores, while the MEDUSA2 computation requires less than five minutes.

3 Results and Discussion

3.1 Initial state of FESOM2.1-REcoM3p: Simulation R_{sedbox}

Generally, the initial FESOM2.1-REcoM3p run (R_{sedbox}) reproduced the global averaged vertical profiles of DIC, alkalinity and the macronutrients DIN and DSi as found in the GLODAPv2 data with their minima at the ocean surface and maxima in greater ocean depth (Large and Yeager, 2009) rather well (Fig. 3). Total global net primary production (NPP) of 37 $\mathrm{PgC\,yr^{-1}}$ is at the lower end of the satellite-based estimates (Gürses et al., 2023, Table 3 and references therein) but comparable to other modelling studies, e.g. 24.5–57.3 $\mathrm{PgC\,yr^{-1}}$ in CMIP6 (Séférian et al., 2020). Diatoms contribute with 12.5 $\mathrm{PgC\,yr^{-1}}$ to this global NPP while the dominant part of 24.5 $\mathrm{PgC\,yr^{-1}}$ is based on small phytoplankton. Carbon export out of the upper 100 m layer is 7.3 $\mathrm{PgC\,yr^{-1}}$. The slightly higher productivity and export found here compared to an NPP of 32.5 $\mathrm{PgC\,yr^{-1}}$ in the base version of FESOM2.1-REcoM3 (Gürses et al., 2023) can be explained by the differences between the model setups: 1) a much coarser spatial resolution of the PI mesh used here and a different forcing data set, which result in differences in resolved physical processes (e.g., circulation and mixing) and thus in the environmental conditions for phytoplankton growth (e.g., light, temperature and nutrient supply); 2) REcoM3p uses a configuration with one zooplankton class whereas the simulations
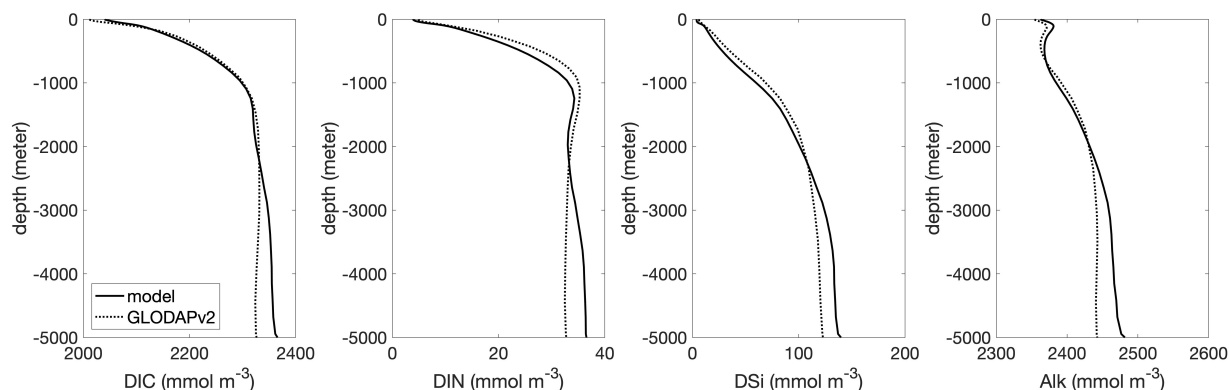
Figure 3. Horizontal averages of DIC, DIN, DSi and alkalinity in R_{sedbox} compared with GLODAPv2 data which are also used as initial concentrations in our simulation.

in Gürses et al. (2023) contained two zooplankton classes; 3) additional iron input from rivers relieves the iron limitation of phytoplankton growth in some regions.

240   Particle fluxes from the ocean bottom layer to the sediment from simulations and reconstructions are summarized in Table 1. The POC flux of $571 \, \mathrm{PgC \, kyr^{-1}}$ that we find in R_{sedbox} is comparable with $500 \, \mathrm{PgC \, kyr^{-1}}$ found in Seiter et al. (2005) and falls within the range of $50–2600 \, \mathrm{PgC \, kyr^{-1}}$ reported by Burdige (2007). It is, however, greater than the commonly cited range of $120–210 \, \mathrm{PgC \, kyr^{-1}}$ (Cartapanis et al., 2018). The simulated POC flux mainly occurs over continental shelves, with $\sim 60\%$ of the total flux into the sediment taking place in waters shallower than $2000 \, \mathrm{m}$. This is qualitatively in agreement

245   with, but quantitatively lower, than most of the estimates (e.g. Burdige, 2007; Dunne et al., 2007), though Muller-Karger et al. (2005) reported about two thirds of POC sinking to the seafloor with a water depth between $50–2000 \, \mathrm{m}$. Models with a coarse resolution do not well resolve physical processes and thus the biological recycling of carbon in shelf regions, likely leading to an unrealistic estimation of POC sinking into and accumulation in sediments. With a very coarse resolution consisting of about 3000 grid cells, the model accomplished its task reasonably well. A total calcite burial of $329 \, \mathrm{PgC \, kyr^{-1}}$ is in line with estimates

250   of $CaCO_3$ burial based on sediment core samples (about $30–300 \, \mathrm{PgC \, kyr^{-1}}$ in shallow waters and $100–150 \, \mathrm{PgC \, kyr^{-1}}$ in deep-sea environments, Cartapanis et al. (2018)). Those estimates suggest a roughly equal distribution between shallow and deep-sea environments, while our model simulates about 10% of the global calcite burial in waters shallower than $1 \, \mathrm{km}$. This is likely caused by the coarse resolution, missing benthic production of $CaCO_3$ (e.g., by coral reefs) and ignoring aragonite completely in the model. Buitenhuis et al. (2019) simulated three pelagic calcifiers and estimated a contribution of aragonite producers to

255   shallow water export of $CaCO_3$ at $100 \, \mathrm{m}$ of at least 33%. Furthermore, coccolithophore and calcifying zooplankton together are reported to contribute to the global carbonate fluxes by $40–60\%$ and the rest of the fluxes remains unexplained (Knecht et al., 2023), which also results in high uncertainty in modelling calcifying organisms and $CaCO_3$ fluxes. The opal flux of $65 \, \mathrm{Tmol \, Si \, yr^{-1}}$ is at the lower end of the data-based estimate of $84 \, \mathrm{Tmol \, Si \, yr^{-1}} \pm 20\%$ (Tréguer et al., 2021).

During the total 2500 simulated years the atmospheric CO_2 concentration rises with time after ocean circulation is stabilised

260   (after $200–300$ years) and reaches a steady state concentration of $293 \, \mathrm{ppm}$ after ca. 2000 years (Fig. 4).

Table 1. Sinking fluxes of POC, calcite and opal onto the top of sediments in different simulations and measurement-based estimates, reported for the global ocean and ocean regions deeper than 1 km. References: 1:Burdige (2007); 2: Cartapanis et al. (2018); 3: Tréguer et al. (2021).

Flux	Unit	R_{sedbox}		$R_{coupled}$		Data	References
		all	>1 km	all	>1 km		
POC	$PgC\,kyr^{-1}$	571	333	501	326	50–2600	(ref. 1, 2)
calcite	$PgC\,kyr^{-1}$	329	295	341	305	shallow: 30–300	(ref. 2)
						deep: 100-150	(ref 2)
opal	$Pmol\,Si\,kyr^{-1}$	65	59	71	64	84±17	(ref. 3)
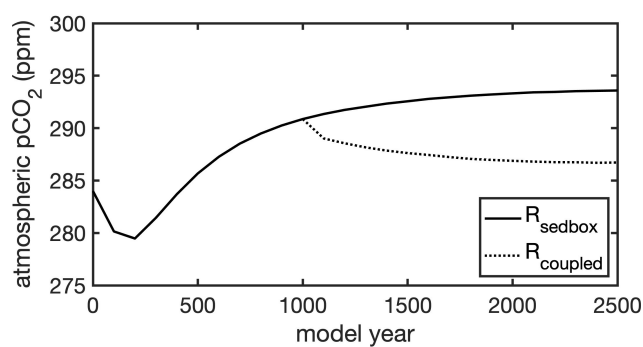
Figure 4. Simulated atmospheric CO_2 during 2500 model years: a FESOM2-REcoM3p simulation with an integrated one-layer sediment (R_{sedbox}) was run for 2500 years; after 1000 years a simulation coupled with MEDUSA2 ($R_{coupled}$) was branched off and run for another 1500 years.

3.2 Initializing MEDUSA2: Simulation R_{medinit}

The weight percentage of sediment composition (Fig. 5) was compared with data compilations of surface sediment composition (Hayes et al., 2021; Seiter et al., 2004). This paper only contains figures of simulated sediment composition and data compilation by Hayes et al. (2021), since Seiter et al. (2004) and Hayes et al. (2021) agree widely.

265   R_{medinit} (Fig. 5, row 1) exhibits high calcite content (up to 99%) in the Atlantic, tropical and subtropical South Pacific as well as the Indian Ocean, and lower values (near zero) in the North Pacific and Southern Ocean. Also, the calcite-rich sediments along the Atlantic mid-ocean ridge are reproduced in the model. This simulated pattern generally agrees well with Hayes et al. (2021) and Seiter et al. (2004). We further compared the pattern and range of sinking fluxes out of the ocean bottom layer in R_{sedbox} (used as input for R_{medinit}) with the flux estimates by Hayes et al. (2021) using spatially-interpolated

270 ^{230}Th-normalized fluxes and spatially-interpolated weight percentage of $CaCO_3$, opal and POC. The model results of $CaCO_3$ agree well with the flux estimates in most of the ocean regions, only values in the eastern equatorial Pacific Ocean are higher by about $1\,\mathrm{g\,cm^{-2}\,kyr^{-1}}$ than in Hayes et al. (2021).

    Opal content (Fig. 5, row 2) is elevated at high latitudes in the North Pacific and North Atlantic Oceans, as well as in the Southern Ocean at the Antarctic Polar Front. This is also seen in the observational data compilation. The opal distribution mainly reflects the diatom productivity (Fig. 6) and opal sinking fluxes. The latter has a similar pattern as ^{230}Th-normalized

275 estimates by Hayes et al. (2021). In coastal regions around Antarctica, however, highest opal fluxes are found in R_{sedbox}. This could lead to a likely overestimation of opal content in sediments, although no observations are available for these areas. The opal belt in the equatorial eastern Pacific is smaller and less pronounced in the model than observed. This is related to the somewhat too strong iron limitation of diatoms in this region in our ocean model.

280   Simulated sediment POC (Fig. 5, row 3) shows a strong contrast between shelf regions and open oceans which is not seen in the data compilation. In large areas of the open ocean and low-latitude shelf regions, the modelled POC content is negligibly low compared with data, whereas in most of the high-latitude shelf regions, it is up to one order of magnitude higher than the measurements. In the eastern equatorial Pacific and the Indian sector of the Southern Ocean the modelled POC has the same order of magnitude as data compilation. A detailed comparison of POC content in the southern hemisphere is not possible due to lack of data. Yet in the comparison of sinking fluxes with estimates from Hayes et al. (2021) we found that the simulated

285 sinking fluxes along the Antarctic coasts are about one order of magnitude higher than the estimates, which likely contributes to overestimate the POC fraction in the sediments. Overall, simulated sinking fluxes of organic matter strongly depend on the resolution of biogeochemical processes in shelf regions which is rather limited in simulations in the PI mesh.
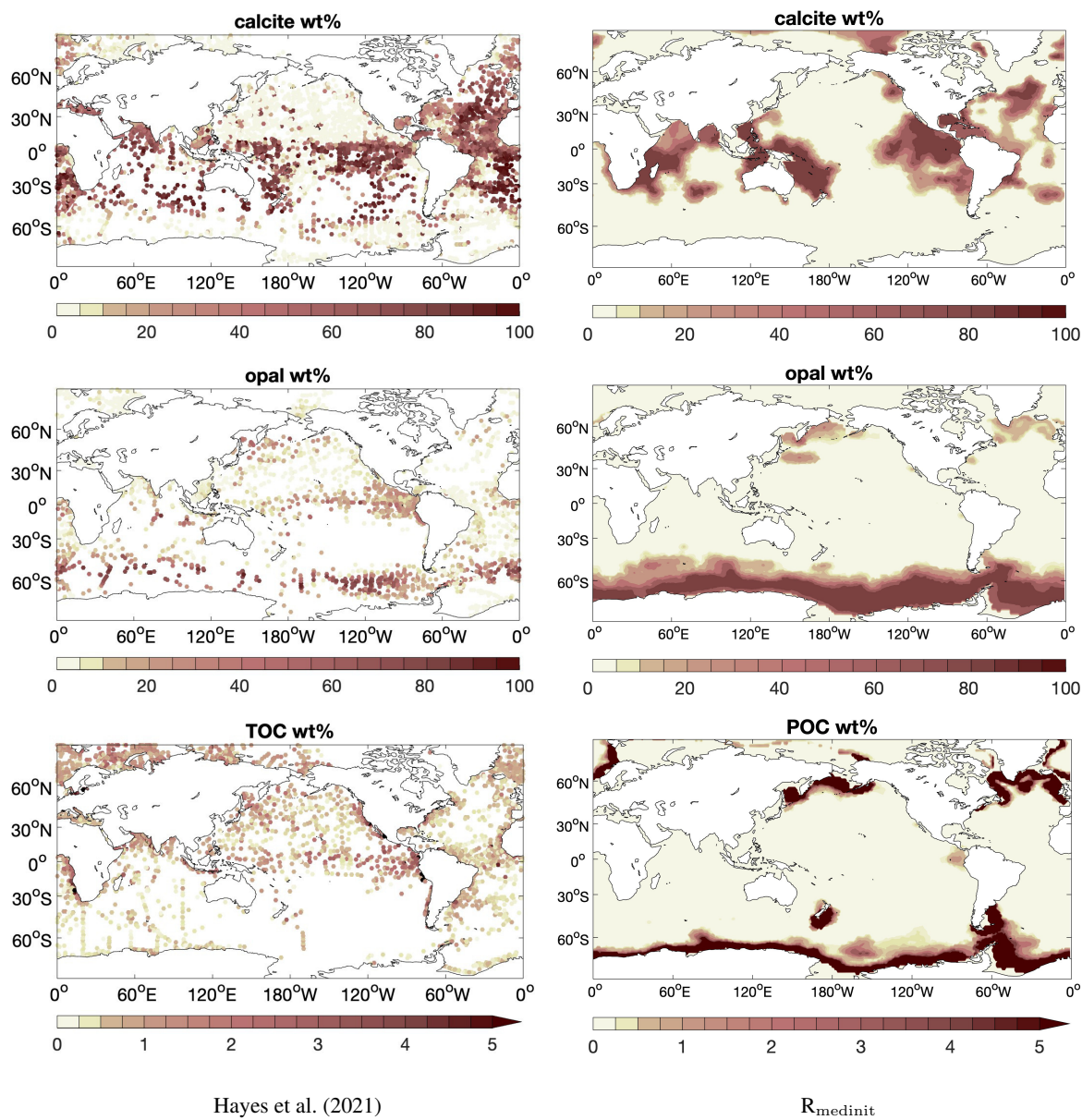
Figure 5. Distribution (weight %) of (row 1) calcite, (row 2) opal and (row 3) particulate organic carbon (POC) in the sediment. Left: data compilation by Hayes et al. (2021); Right: results from simulation $R_{medinit}$.
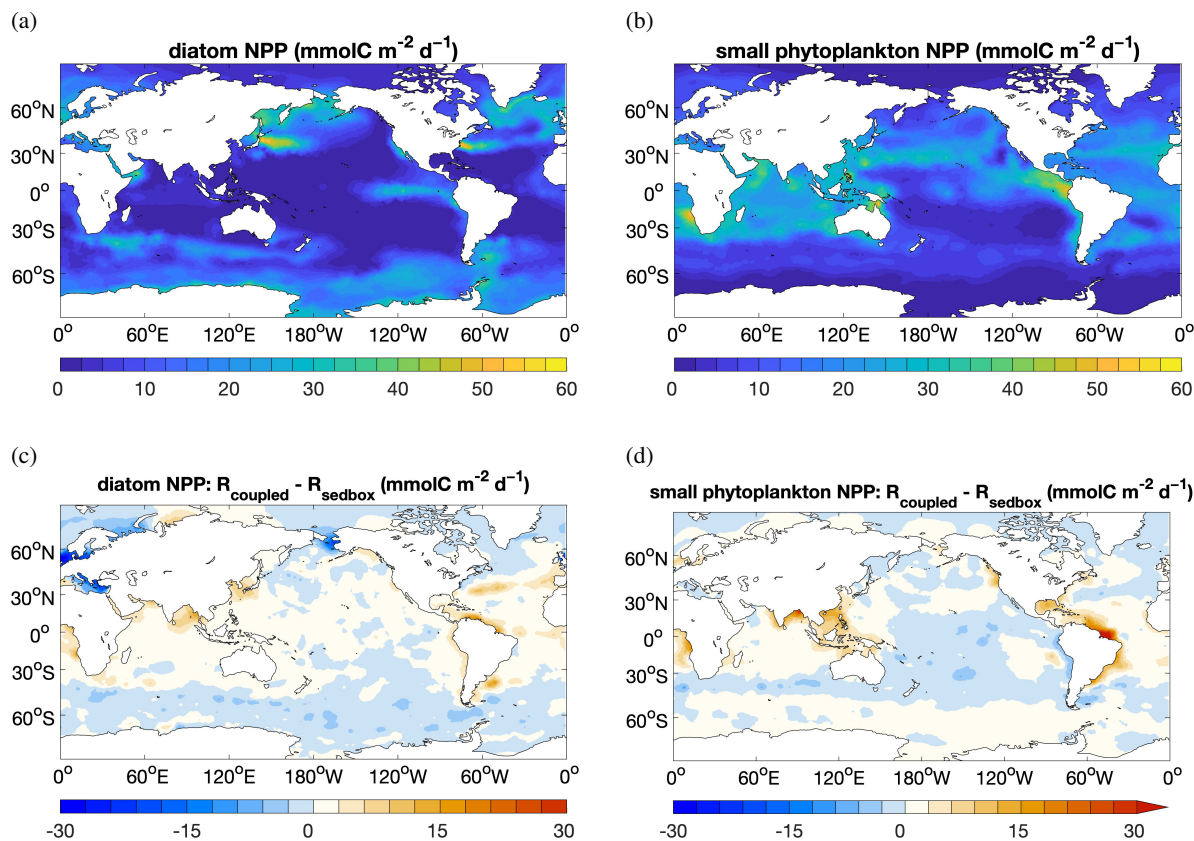
Figure 6. NPP (mmolC m^{-2} day^{-1}) of (a) diatoms and (b) small phytoplankton in R$_{\text{sedbox}}$ and the difference in NPP (c,d) for the two simulations (R$_{\text{coupled}}$–R$_{\text{sedbox}}$).

3.3 The coupled simulation R$_{\text{coupled}}$

290   **3.3.1 Impact on productivity and nutrient supply**

Marine primary production in the coupled simulation R$_{\text{coupled}}$ remains nearly unchanged when compared with R$_{\text{sedbox}}$, with a slight increase from 37.0 to 38.3 PgC yr^{-1} with 0.5 PgC yr^{-1} of the increase contributed by diatoms and 0.8 PgC yr^{-1} by small phytoplankton. The spatial distribution of NPP differences between the coupled simulation and R$_{\text{sedbox}}$ (Fig. 6) reveals higher productivity by both diatoms and small phytoplankton in coastal regions with large riverine input of nutrients (DIN and DSi,

295   Fig. 7), which were not considered for R$_{\text{sedbox}}$.

     Nutrient supply in the simulations using MEDUSA2 or the one-layer sediment differs in two ways. First, the total diagenetic flux of nutrients from the sediment to the ocean is lower when using MEDUSA2 (Table 2), since particles sinking into sediment can be stored there: a part is degraded and dissolved in the reactive layer and comes back to bottom water by diffusion, while the rest is buried in the deeper sediments (Munhoven, 2021). This storage and burial delay nutrient recycling and reduce the
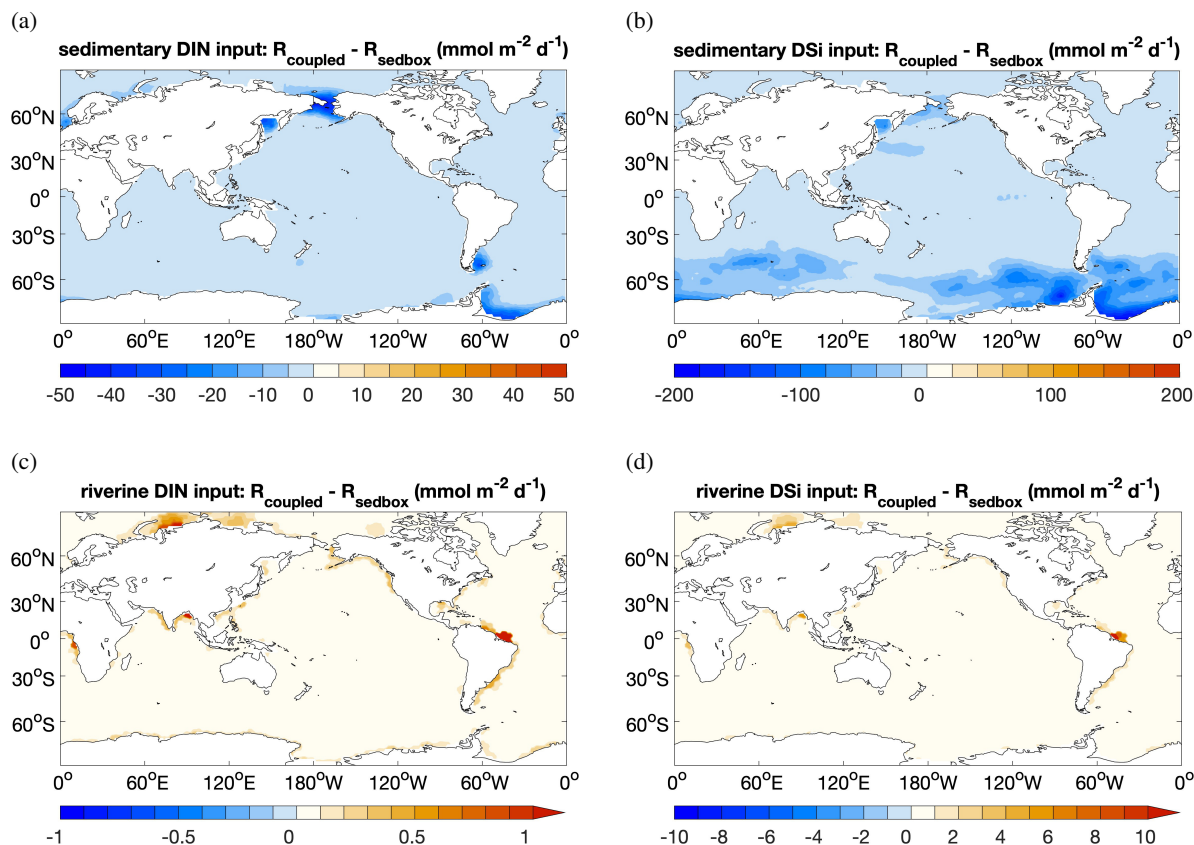
Figure 7. Decrease of sedimentary input of (a) DIN and (b) DSi in $R_{coupled}$ compared to R_{sedbox}; additional riverine input of (c) DIN and (d) DSi in coupled simulations $R_{coupled}$ (mmol m^{-2} day^{-1}). Change in sedimentary input of DFe has an identical spatial pattern as DIN since the iron source is calculated based on DIN source with a constant Fe:N ratio.

300 sedimentary nutrient source when compared to the full degradation and dissolution which takes places in the one-box sediment. A part of the lower sedimentary input of N in $R_{coupled}$ is also explained by denitrification in sediments which oxidizes organic compounds and ultimately transforms DIN into N$_2$. Based on processes considered in the model, a small fraction of 2% in 1 kyr of N is lost from the mass balance in the ocean-sediment system. To conserve the mass of N, an additional N source should be considered in future work, e.g. via N$_2$-fixation or a higher input from rivers. Second, the current riverine source of

305 nutrients considered in coupled simulations is estimated based on the burial flux from the reactive sediment layer to the core layer in MEDUSA2. This additional source brings nutrients directly into surface waters near river mouths (Fig. 7). As a result, diatom productivity shows a clear decrease in the North Sea and Bering Sea (Fig. 6c) where DIN, DSi and DFe from sediments are all significantly reduced (Fig. 7a and b) and no riverine input can cover the loss (Fig. 7c and d).

   For Si, the total riverine supply is higher than the reduction of sedimentary input (Table 2: 11 vs. 5.1 Tmol Si year^{-1}),

310 while for N, it cannot compensate the decline in sediment source (2.4 vs. 5.4 Tmol N year^{-1}). However, the nutrients supplied by rivers are directly available for phytoplankton living in surface waters and can still induce phytoplankton growth in areas

adjacent to river mouths (Fig. 6c and d), particularly in regions where sedimentary input does not change much (e.g. tropical and subtropical regions). The sedimentary source of iron strongly decreases as well (Table 2), however, the intensity of iron limitation for phytoplankton does not change significantly, since the riverine source is much higher and covers most of the

315   regions where sedimentary input becomes smaller in $R_{coupled}$.

Table 2. Fluxes averaged over the last 50 years of the simulations. Positive fluxes are into the ocean or into sediments. Continued on next page. Note that the units here are Tmol year^{-1}, not Pg year^{-1}.

	Ocean balance	R_{sedbox}	$R_{coupled}$
	riverine input	0	+27
	diffusive flux out of sediment	+76.4	+47.6
	seafloor deposition (POC)	−48.0	−44.4
C	seafloor deposition (Calc)	−27.4	−28.8
	air-sea gas exchange	−0.9	+0.1
(Tmol year^{-1})	Sediment balance		
	seafloor deposition (POC)	+48.0	+44.4
	seafloor deposition (Calc)	+27.4	+28.8
	diffusive flux out of sediment	−76.4	−47.6
	burial (POC)	0	−16.3
	burial (Calc)	0	−7.9
	Ocean balance		
	riverine input	0	+24
	diffusive flux out of sediment	+47.9	+35.8
Alk	seafloor deposition (POM)	+7.5	+6.5
	seafloor deposition (Calc)	−54.8	−57.5
(Tmol year^{-1})	Sediment balance		
	seafloor deposition (POM)	−7.5	−6.5
	seafloor deposition (Calc)	+54.8	+57.5
	diffusive flux out of sediment	−47.9	−35.8
	sedimentary denitrification	0	−0.7
	burial (POM)	0	+2.5
	burial (Calc)	0	−15.8

	Ocean balance		
	riverine input	0	+2.4
	diffusive NO_3 flux out of sediment	+7.2	+1.8
N	seafloor deposition	−7.1	−6.0
	Sediment balance		
(Tmol year^{-1})	seafloor deposition	+7.1	+6.0
	diffusive NO_3 flux out of sediment	−7.2	−1.8
	sedimentary denitrification	0	−1.7
	burial (POM)	0	−2.4
	Ocean balance		
	riverine input	0	+11.0
Si	diffusive flux out of sediment	+65.8	+60.7
	seafloor deposition	−64.8	−71.8
(Tmol year^{-1})	Sediment balance		
	seafloor deposition	+64.8	+71.8
	diffusive flux out of sediment	−65.8	−60.7
	burial (opal)	0	−11.0
Fe	dust	+5.8	+5.8
(Gmol year^{-1})	rivers	+2.6	+2.6
	diffusive flux out of sediment	+1.1	+0.3

3.3.2 Changes in sediment contents

After the 1500-year coupled simulation the contents of calcite, opal and POC are altered to different extents from the initial values in R_{medinit} (Fig. 8). Sediment content of calcite increases in most of regions that are strongly influenced by riverine nutrient input (Fig. 7c). This pattern generally follows the pattern of NPP change by small phytoplankton (Fig. 6d). Opal content in the sediment surface is lowered mainly in areas in the Southern Ocean, following changes in diatom productivity. In these upwelling regions, DSi supply is reduced due to the decrease of global sedimentary input (Fig. 7b). Differences in sedimentary POC between the two simulations are negligibly small.

3.3.3 Impact on atmospheric CO$_2$ and carbon storage

The oceanic carbon pools moved towards equilibrium concentrations during R_{coupled} by adjusting the gas exchange and the fluxes between ocean and sediment. The atmospheric CO_2 in R_{coupled} declined and stabilised at 287 ppm after 1500 years with a just slightly positive net air-sea gas exchange (Table 2), which is close to the pre-industrial CO_2 value of 284.3 ppm used initially in R_{sedbox}. Compared to R_{sedbox}, the ocean contained about 94 Pg more DIC in R_{coupled}. Furthermore, in the coupled simulation the sediment surface layer accumulated 402 PgC, mainly as calcite but with a 5% contribution from POC, while in the version with the one-box sediment the reservoir sizes of carbon in the sediment were close to zero (Table 3). This shift of carbon between reservoirs (atmosphere, ocean and sediment) is explained by the long-term storage of material in the sediments. Here, the atmospheric CO_2 content is indirectly affected by the changing marine alkalinity inventory, which subsequently determines how DIC is distributed into its three species CO_2, HCO_3^-, and CO_3^{2-}, from which only CO_2 can exchange with the atmosphere (Zeebe and Wolf-Gladrow, 2001). The riverine input of DIC and Alk exceeds the sedimentary burial loss by 2.8 TmolC yr^{-1} and 5.7 Tmol Alk yr^{-1}, resulting in an increase of the carbon and alkalinity inventories of about 0.1% and 0.2% kyr^{-1}, which slightly affects the change in carbon reservoirs as well.

Table 3. Marine carbon reservoirs (PgC) in our two simulations, averaged over the last 50 years.

Reservoir	R_{sedbox}	R_{coupled}
DIC	35568	35662
DOC	650	650
POC	2	2
Sediment POC	<1	21
Sediment calcite	<1	381

In R_{coupled}, the fluxes into the ocean (CO_2 uptake, riverine input and diffusion of DIC from sediment) and out of the ocean (outgassing and sinking into sediment) are not completely in balance. One reason is that the mass conservation is violated by the asynchronous coupling, i.e., exchange between parts of the coupled model is temporally shifted. This effect is clearly seen in the changes of the Si inventory in R_{coupled}. The only Si flux out of the ocean-sediment system is the sediment burial of
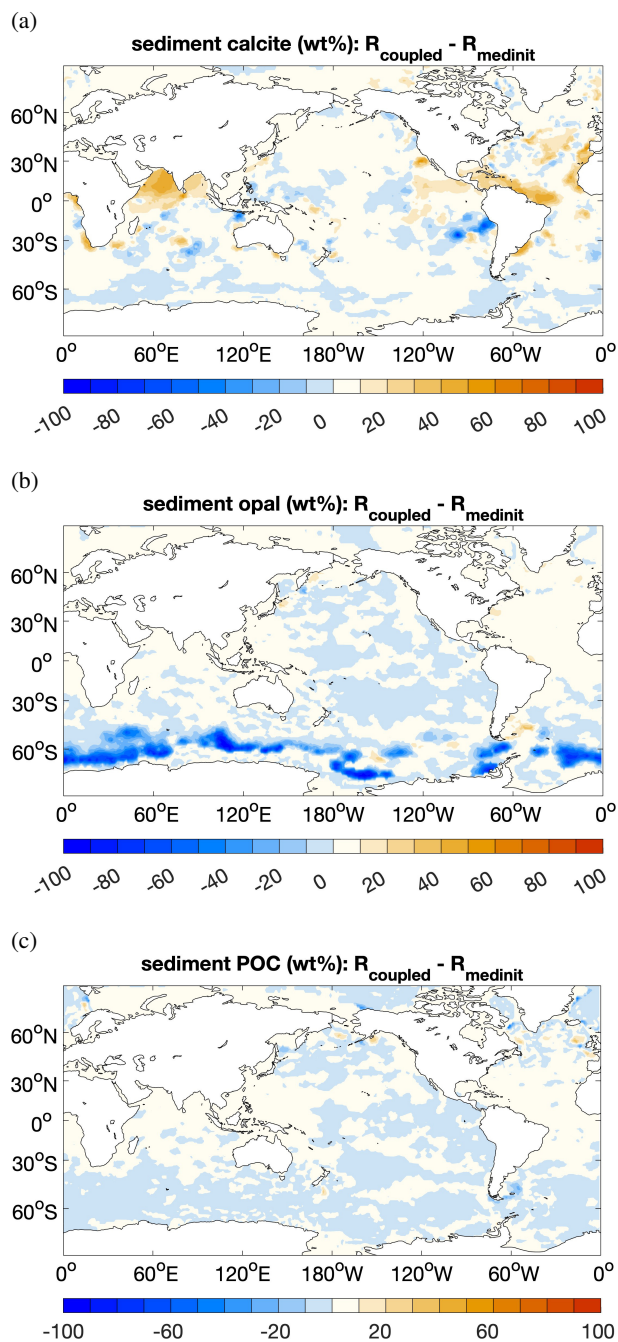
Figure 8. Difference of (a) calcite, (b) opal and (c) POC (weight %) of the reactive sedimentary layer ($R_{coupled} - R_{medinit}$).

opal. In our coupled simulation the riverine input of DSi into FESOM2.1-REcoM3p is determined from the sediment burial of opal calculated in MEDUSA2. Thus, the silicon cycle is a closed system and variations in the silicon inventory with time can

only be explained by temporal offsets of ocean and sediment processes. We found an increase of total silicon by 0.8% from the beginning of $R_{coupled}$ to the end of 1500 model years, indicating a small impact of the offline coupling itself on the mass conservation. Compared to R_{sedbox}, however, the total Si inventory of the ocean and the reactive sediment is larger by +16%

345 due to the filling up of the sediments in the 100,000 years long initialization of MEDUSA $R_{medinit}$. This results in a larger total inventory of carbon in the atmosphere-ocean-sediment system in $R_{coupled}$ than in R_{sedbox}, indicating that a significant part of the marine carbon reservoir size is missing in models without reasonable representations of the sediments.

4   Conclusions

This paper documented the coupling of the sediment model MEDUSA2 to the marine biogeochemical model FESOM2.1-
350 REcoM3. The coupling was realized via file exchange, the size of the annual fluxes that exchange material between the bottom of the ocean and the sedimentary surface, was updated every 50 years. Results from a coupled simulation in a coarse resolution were presented, while a simulation with a much simpler one-layer sediment was used as reference for comparisons.

The coupled simulation reasonably reproduced the distribution of DIC, Alk, nutrients and total global primary production found in observational data products. While the sediment content of calcite generally agrees well with measurements, the coarse
355 resolution and some missing processes in the ecosystem model lead to some mismatches between simulated and observed sediment content of POC and opal. Nutrient supply from sediments is lower in the coupled simulation than in the application with the one-layer sediment, particularly for nitrogen. However, the biological pump is not significantly affected by this decrease, since the additional riverine input compensates it by bringing nutrients directly into the surface ocean. Changes in these two sources of nutrients lead to changes in distribution patterns of diatoms and small phytoplankton. A shift of carbon from the
360 atmosphere to the ocean and sediment reservoir has been found explaining a decrease in atmospheric CO_2 by ∼6 ppm between the coupled and the reference simulations.

Mass conservation in the coupled model is only slightly violated through the asynchronous coupling. We found an increase of total silicon by 0.8% during the 1500 model years in the coupled simulation. A net nitrogen loss of 1.7 Tmol N year^{-1} is caused by denitrification in MEDUSA2 and violate the mass conservation of N by 2% in 1000 years. An additional N source
365 for FESOM2.1-REcoM3, e.g. N_2 fixation, needs to be considered to compensate this offset in future work.

Our MEDUSA2 application is being further developed for parallel processing. With that, FESOM2.1-REcoM3 can be run with MEDUSA2 in higher spatial resolution for a better presentation of shelf regions. A MEDUSA2 application including carbon isotopes is under development. Currently, REcoM3p is being used in the Earth System Model AWI-ESM2 (Shi et al., 2023) to explore the role of changes in the carbon cycle during the last glacial cycle. The approach of coupled ocean-sediment
370 models presented in this paper and further developments mentioned above will contribute considerably to investigation of the transient changes in the carbon storage of the atmosphere-ocean-sediment system and its feedbacks to Earth's cimate.

Code and data availability.   The source code is available at https://doi.org/10.5281/zenodo.8315239.

Author contributions. YY and CV performed the model setup with help from GM, MB and ÖG. YY conducted the simulations and prepared the manuscript with contributions from all co-authors.

375 *Competing interests.* No competing interests are present.

Acknowledgements. YY, PK, CV and MB are supported by the German Federal Ministry of Education and Research (BMBF), as Research for Sustainability initiative (FONA); www.fona.de through the PalMod project (grant number: 01LP1919A). M.B. is additionally funded through DFG-ANR project MARCARA. JH and ÖG were funded by the Initiative and Networking Fund of the Helmholtz Association (Helmholtz Young Investigator Group Marine Carbon and Ecosystem Feedbacks in the Earth System [MarESys], grant number VH-NG-
380 1301). Financial support for GM's work on MEDUSA was provided by the Belgian Fund for Scientific Research – F.R.S.-FNRS (project SERENATA, grant no. CDR J.0123.19). GM is a Research Associate with the Belgian Fund for Scientific Research – F.R.S.-FNRS.

References

Albani, S., Mahowald, N. M., Perry, A. T., Scanza, R. A., Zender, C. S., Heavens, N. G., Maggi, V., Kok, J. F., and Otto-Bliesner, B. L.: Improved Dust Representation in the Community Atmosphere Model, Journal of Advances in Modeling Earth Systems, 6, 541–570, https://doi.org/10.1002/2013MS000279, 2014.

Archer, D., Kheshgi, H., and Maier-Reimer, E.: Multiple timescales for neutralization of fossil fuel CO_2, Geophysical Research Letters, 24, 405–408, https://doi.org/10.1029/97GL00168, 1997.

Archer, D., Eby, M., Brovkin, V., Ridgwell, A., Cao, L., Mikolajewicz, U., Caldeira, K., Matsumoto, K., Munhoven, G., Montenegro, A., and Tokos, K.: Atmospheric Lifetime of Fossil Fuel Carbon Dioxide, Annual Review of Earth and Planetary Sciences, 37, 117–134, https://doi.org/10.1146/annurev.earth.031208.100206, 2009.

Aumont, O., Ethé, C., Tagliabue, A., Bopp, L., and Gehlen, M.: PISCES-v2: An Ocean Biogeochemical Model for Carbon and Ecosystem Studies, Geoscientific Model Development, 8, 2465–2513, https://doi.org/10.5194/gmd-8-2465-2015, 2015.

Berner, R. A.: Biogeochemical cycles of carbon and sulfur and their effect on atmospheric oxygen over phanerozoic time, Palaeogeography, Palaeoclimatology, Palaeoecology, 75, 97–122, https://doi.org/10.1016/0031-0182(89)90186-7, the Long Term Stability of the Earth System, 1989.

Börker, J., Hartmann, J., Amann, T., Romero-Mujalli, G., Moosdorf, N., and Jenkins, C.: Chemical Weathering of Loess and Its Contribution to Global Alkalinity Fluxes to the Coastal Zone During the Last Glacial Maximum, Mid-Holocene, and Present, Geochemistry, Geophysics, Geosystems, 21, e2020GC008922, https://doi.org/10.1029/2020GC008922, 2020.

Broecker, W. S. and Peng, T.-H.: The role of $CaCO_3$ compensation in the glacial to interglacial atmospheric CO_2 change, Global Biogeochemical Cycles, 1, 15–29, 1987.

Brovkin, V., Ganopolski, A., Archer, D., and Munhoven, G.: Glacial CO_2 cycle as a succession of key physical and biogeochemical processes, Climate of the Past, 8, 251–264, https://doi.org/10.5194/cp-8-251-2012, 2012.

Buitenhuis, E. T., Le Quéré, C., Bednaršek, N., and Schiebel, R.: Large Contribution of Pteropods to Shallow CaCO3 Export, Global Biogeochemical Cycles, 33, 458–468, https://doi.org/10.1029/2018GB006110, 2019.

Burdige, D. J.: Preservation of Organic Matter in Marine Sediments: Controls, Mechanisms, and an Imbalance in Sediment Organic Carbon Budgets?, Chemical Reviews, 107, 467–485, https://doi.org/10.1021/cr050347q, 2007.

Butzin, M., Ye, Y., Völker, C., Gürses, O., Hauck, J., and Köhler, P.: Carbon isotopes in the marine biogeochemistry model FESOM2.1-REcoM3, EGUsphere, 2023, 1–36, https://doi.org/10.5194/egusphere-2023-1718, 2023.

Cartapanis, O., Galbraith, E. D., Bianchi, D., and Jaccard, S. L.: Carbon Burial in Deep-Sea Sediment and Implications for Oceanic Inventories of Carbon and Alkalinity over the Last Glacial Cycle, Clim. Past, 14, 1819–1850, https://doi.org/10.5194/cp-14-1819-2018, 2018.

Catubig, N. R., Archer, D. E., François, R., deMenocal, P., Howard, W., and Yu, E.-F.: Global deep-sea burial rate of calcium carbonate during the last glacial maximum, Paleoceanography, 13, 298–310, https://doi.org/10.1029/98PA00609, 1998.

de Baar, H. J. W. and de Jong, J.: Distributions, Sources and Sinks of Iron in Seawater, in: The Biogeochemistry of Iron in Seawater, edited by Turner, D. R. and Hunter, K. A., vol. 7 of *IUPAC Ser. Anal. Phys. Chem. Environ. Syst.*, pp. 123–253, John Wiley & Sons, 2001.

Dunne, J. P., Sarmiento, J. L., and Gnanadesikan, A.: A synthesis of global particle export from the surface ocean and cycling through the ocean interior and on the seafloor, Global Biogeochemical Cycles, 21, GB4006, https://doi.org/10.1029/2006GB002907, 2007.

Dunne, J. P., Hales, B., and Toggweiler, J. R.: Global calcite cycling constrained by sediment preservation controls, Global Biogeochemical Cycles, 26, GB3023, https://doi.org/10.1029/2010GB003935, 2012.

420 Friedlingstein, P., O'Sullivan, M., Jones, M. W., Andrew, R. M., Gregor, L., Hauck, J., Le Quéré, C., Luijkx, I. T., Olsen, A., Peters, G. P., Peters, W., Pongratz, J., Schwingshackl, C., Sitch, S., Canadell, J. G., Ciais, P., Jackson, R. B., Alin, S. R., Alkama, R., Arneth, A., Arora, V. K., Bates, N. R., Becker, M., Bellouin, N., Bittig, H. C., Bopp, L., Chevallier, F., Chini, L. P., Cronin, M., Evans, W., Falk, S., Feely, R. A., Gasser, T., Gehlen, M., Gkritzalis, T., Gloege, L., Grassi, G., Gruber, N., Gürses, Ö., Harris, I., Hefner, M., Houghton, R. A., Hurtt, G. C., Iida, Y., Ilyina, T., Jain, A. K., Jersild, A., Kadono, K., Kato, E., Kennedy, D., Klein Goldewijk, K., Knauer, J., Korsbakken, J. I.,

425 Landschützer, P., Lefèvre, N., Lindsay, K., Liu, J., Liu, Z., Marland, G., Mayot, N., McGrath, M. J., Metzl, N., Monacci, N. M., Munro, D. R., Nakaoka, S.-I., Niwa, Y., O'Brien, K., Ono, T., Palmer, P. I., Pan, N., Pierrot, D., Pocock, K., Poulter, B., Resplandy, L., Robertson, E., Rödenbeck, C., Rodriguez, C., Rosan, T. M., Schwinger, J., Séférian, R., Shutler, J. D., Skjelvan, I., Steinhoff, T., Sun, Q., Sutton, A. J., Sweeney, C., Takao, S., Tanhua, T., Tans, P. P., Tian, X., Tian, H., Tilbrook, B., Tsujino, H., Tubiello, F., van der Werf, G. R., Walker, A. P., Wanninkhof, R., Whitehead, C., Willstrand Wranne, A., Wright, R., Yuan, W., Yue, C., Yue, X., Zaehle, S., Zeng, J., and Zheng, B.:

430 Global Carbon Budget 2022, Earth System Science Data, 14, 4811–4900, https://doi.org/10.5194/essd-14-4811-2022, 2022.

Garcia, H. E., Locarnini, R. A., Boyer, T. P., Antonov, J. I., Baranova, O. K., Zweng, M. M., Reagan, J. R., and Johnson, D. R.: World Ocean Atlas 2013, Volume 4: Dissolved Inorganic Nutrients (Phosphate, Nitrate, Silicate). S. Levitus, Ed., A. Mishonov Technical Ed., Tech. rep., NOAA Atlas NESDIS 76, 2014.

Garcia, H. E., Weathers, K. W., Paver, C. R., Smolyar, I., Boyer, T. P., Locarnini, R. A., Zweng, M. M., Mishonov, A. V., Baranova,

435 O. K., Seidov, D., and Reagan, J. R.: World Ocean Atlas 2018, Volume 3: Dissolved Oxygen, Apparent Oxygen Utilization, and Oxygen Saturation. A. Mishonov Technical Editor, Tech. rep., NOAA Atlas NESDIS 83, 2019.

Gürses, O., Oziel, L., Karakuş, O., Sidorenko, D., Völker, C., Ye, Y., Zeising, M., Butzin, M., and Hauck, J.: Ocean biogeochemistry in the coupled ocean–sea ice–biogeochemistry model FESOM2.1–REcoM3, Geoscientific Model Development, 16, 4883–4936, https://doi.org/10.5194/gmd-16-4883-2023, 2023.

440 Hayes, C. T., Costa, K. M., Anderson, R. F., Calvo, E., Chase, Z., Demina, L. L., Dutay, J.-C., German, C. R., Heimbürger-Boavida, L.-E., Jaccard, S. L., Jacobel, A., Kohfeld, K. E., Kravchishina, M. D., Lippold, J., Mekik, F., Missiaen, L., Pavia, F. J., Paytan, A., Pedrosa-Pamies, R., Petrova, M. V., Rahman, S., Robinson, L. F., Roy-Barman, M., Sanchez-Vidal, A., Shiller, A., Tagliabue, A., Tessin, A. C., Van Hulten, M., and Zhang, J.: Global Ocean Sediment Composition and Burial Flux in the Deep Sea, Global Biogeochemical Cycles, 35, e2020GB006769, https://doi.org/10.1029/2020GB006769, 2021.

445 Hedges, J. I. and Keil, R. G.: Sedimentary organic matter preservation : an assessment and speculative synthesis, Marine Chemistry, 49, 81–115, https://doi.org/10.1016/0304-4203(95)00008-F, 1995.

Heinze, C., Maier-Reimer, E., Winguth, A. M. E., and Archer, D.: A Global Oceanic Sediment Model for Long-Term Climate Studies, Global Biogeochemical Cycles, 13, 221–250, https://doi.org/10.1029/98GB02812, 1999.

Himstedt, K.: Multiple Execution of the Same MPI Application to Exploit Parallelism at Hotspots with Minimal Code Changes: A Case

450 Study with FESOM2-Iceberg and FESOM2-REcoM, EGUsphere, 2023, 1–27, https://doi.org/10.5194/egusphere-2023-756, 2023.

Keppler, L., Landschützer, P., Gruber, N., Lauvset, S. K., and Stemmler, I.: Seasonal Carbon Dynamics in the Near-Global Ocean, Global Biogeochemical Cycles, 34, e2020GB006571, https://doi.org/10.1029/2020GB006571, 2020.

Knecht, N. S., Benedetti, F., Hofmann Elizondo, U., Bednaršek, N., Chaabane, S., de Weerd, C., Peijnenburg, K. T. C. A., Schiebel, R., and Vogt, M.: The Impact of Zooplankton Calcifiers on the Marine Carbon Cycle, Global Biogeochemical Cycles, 37, e2022GB007685,

455 https://doi.org/10.1029/2022GB007685, 2023.

Köhler, P.: Anthropogenic CO_2 of high emission scenario compensated after 3500 years of ocean alkalinization with an annually constant dissolution of 5 Pg of olivine, Frontiers in Climate, 2, 575744, https://doi.org/10.3389/fclim.2020.575744, 2020.

Köhler, P. and Munhoven, G.: Late Pleistocene carbon cycle revisited by considering solid Earth processes, Paleoceanography and Paleoclimatology, 35, e2020PA004020, https://doi.org/10.1029/2020PA004020, 2020.

460 Kriest, I. and Oschlies, A.: Swept under the Carpet: Organic Matter Burial Decreases Global Ocean Biogeochemical Model Sensitivity to Remineralization Length Scale, Biogeosciences, 10, 8401–8422, https://doi.org/10.5194/bg-10-8401-2013, 2013.

Kurahashi-Nakamura, T., Paul, A., Munhoven, G., Merkel, U., and Schulz, M.: Coupling of a Sediment Diagenesis Model (MEDUSA) and an Earth System Model (CESM1.2): A Contribution toward Enhanced Marine Biogeochemical Modelling and Long-Term Climate Simulations, Geoscientific Model Development, 13, 825–840, https://doi.org/10.5194/gmd-13-825-2020, 2020.

465 Lan, X., Tans, P., and K.W., T.: Trends in globally-averaged CO_2 determined from NOAA Global Monitoring Laboratory measurements. Version 2023-06, https://doi.org/10.15138/9N0H-ZH07, last access: 31th August 2023, 2023.

Large, W. G. and Yeager, S. G.: The Global Climatology of an Interannually Varying Air-Sea Flux Data Set, Climate Dynamics, 33, 341–364, https://doi.org/10.1007/s00382-008-0441-3, 2009.

Lauvset, S. K., Key, R. M., Olsen, A., van Heuven, S., Velo, A., Lin, X., Schirnick, C., Kozyr, A., Tanhua, T., Hoppema, M., Jutterström, S.,
470 Steinfeldt, R., Jeansson, E., Ishii, M., Perez, F. F., Suzuki, T., and Watelet, S.: A New Global Interior Ocean Mapped Climatology: The 1×1 GLODAP Version 2, Earth System Science Data, 8, 325–340, https://doi.org/10.5194/essd-8-325-2016, 2016.

Meinshausen, M., Vogel, E., Nauels, A., Lorbacher, K., Meinshausen, N., Etheridge, D., Fraser, P., Montzka, S. A., Rayner, P., Trudinger, C., Krummel, P., Beyerle, U., Cannadell, J. G., Daniel, J. S., Enting, I., Law, R. M., O'Doherty, S., Prinn, R. G., Reimann, S., Rubino, M., Velders, G. J. M., Vollmer, M. K., and Weiss, R.: Historical greenhouse gas concentrations for climate modelling (CMIP6), Geoscientific
475 Model Development, 10, 2057–2116, https://doi.org/10.5194/gmd-10-2057-2017, 2017.

Moreira Martinez, S., Roche, D. M., Munhoven, G., and Waelbroeck, C.: Coupling MEDUSA sediment model to iLOVECLIM (v1.1β) Earth system model, in: 12th International Conference on Paleoceanography (ICP12)., pp. P–368, Utrecht (NL), http://icp12.uu.nl/wp-content/uploads/2016/08/Poster-abstracts-sessie-3.pdf, 2016.

Muller-Karger, F. E., Varela, R., Thunell, R., Luers sen, R., Hu, C., and Walsh, J. J.: The importance of continental margins in the global
480 carbon cycle, Geophysical Research Letters, 32, L01602, https://doi.org/10.1029/2004GL021346, 2005.

Munhoven, G.: Glacial–Interglacial Rain Ratio Changes: Implications for Atmospheric and Ocean–Sediment Interaction, Deep Sea Research Part II: Topical Studies in Oceanography, 54, 722–746, https://doi.org/10.1016/j.dsr2.2007.01.008, 2007.

Munhoven, G.: Model of Early Diagenesis in the Upper Sediment with Adaptable Complexity – MEDUSA (v. 2): A Time-Dependent Biogeochemical Sediment Module for Earth System Models, Process Analysis and Teaching, Geoscientific Model Development, 14,
485 3603–3631, https://doi.org/10.5194/gmd-14-3603-2021, 2021.

Sarmiento, J. L. and Gruber, N.: Ocean Biogeochemical Dynamics, Princeton University Press, https://doi.org/10.2307/j.ctt3fgxqx, 2006.

Sarmiento, J. L., Dunne, J., Gnanadesikan, A., Key, R. M., Matsumoto, K., and Slater, R.: A new estimate of the $CaCO_3$ to organic carbon export ratio, Global Biogeochemical Cycles, 16, 1107, https://doi.org/10.1029/2002GB001919, 2002.

Scholz, P., Sidorenko, D., Gurses, O., Danilov, S., Koldunov, N., Wang, Q., Sein, D., Smolentseva, M., Rakowsky, N., and Jung, T.: Assess-
490 ment of the Finite-volumE Sea Ice-Ocean Model (FESOM2.0) – Part 1: Description of Selected Key Model Elements and Comparison to Its Predecessor Version, Geoscientific Model Development, 12, 4875–4899, https://doi.org/10.5194/gmd-12-4875-2019, 2019.

Scholz, P., Sidorenko, D., Danilov, S., Wang, Q., Koldunov, N., Sein, D., and Jung, T.: Assessment of the Finite-VolumE Sea Ice–Ocean Model (FESOM2.0) – Part 2: Partial Bottom Cells, Embedded Sea Ice and Vertical Mixing Library CVMix, Geoscientific Model Development, 15, 335–363, https://doi.org/10.5194/gmd-15-335-2022, 2022.

495 Schourup-Kristensen, V., Sidorenko, D., Wolf-Gladrow, D. A., and Völker, C.: A skill assessment of the biogeochemical model REcoM2 coupled to the Finite Element Sea-Ice Ocean Model (FESOM 1.3), Geosci. Model Dev., 7, 2769–2802, https://doi.org/10.5194/gmd-7-2769-2014, 2014.

Séférian, R., Berthet, S., Yool, A., Palmiéri, J., Bopp, L., Tagliabue, A., Kwiatkowski, L., Aumont, O., Christian, J., Dunne, J., Gehlen, M., Ilyina, T., John, J. G., Li, H., Long, M. C., Luo, J. Y., Nakano, H., Romanou, A., Schwinger, J., Stock, C., Santana-Falcón, Y., Takano, Y.,

500 Tjiputra, J., Tsujino, H., Watanabe, M., Wu, T., Wu, F., and Yamamoto, A.: Tracking Improvement in Simulated Marine Biogeochemistry Between CMIP5 and CMIP6, Current Climate Change Reports, 6, 95–119, https://doi.org/10.1007/s40641-020-00160-0, 2020.

Seiter, K., Hensen, C., Schröter, J., and Zabel, M.: Organic Carbon Content in Surface Sediments — Defining Regional Provinces, Deep Sea Research Part I: Oceanographic Research Papers, 51, 2001–2026, https://doi.org/10.1016/j.dsr.2004.06.014, 2004.

Seiter, K., Hensen, C., and Zabel, M.: Benthic carbon mineralization on a global scale, Global Biogeochemical Cycles, 19,

505 https://doi.org/10.1029/2004GB002225, 2005.

Shi, X., Cauquoin, A., Lohmann, G., Jonkers, L., Wang, Q., Yang, H., Sun, Y., and Werner, M.: Simulated stable water isotopes during the mid-Holocene and pre-industrial using AWI-ESM-2.1-wiso, Geoscientific Model Development Discussions, 2023, 1–39, https://doi.org/10.5194/gmd-2023-68, 2023.

Steele, M., Morley, R., and Ermold, W.: PHC: A Global Ocean Hydrography with a High-Quality Arctic Ocean, Journal of Climate, 14,

510 2079–2087, https://doi.org/10.1175/1520-0442(2001)014<2079:PAGOHW>2.0.CO;2, 2001.

Tréguer, P. J., Sutton, J. N., Brzezinski, M., Charette, M. A., Devries, T., Dutkiewicz, S., Ehlert, C., Hawkings, J., Leynaert, A., Liu, S. M., Llopis Monferrer, N., López-Acosta, M., Maldonado, M., Rahman, S., Ran, L., and Rouxel, O.: Reviews and Syntheses: The Biogeochemical Cycle of Silicon in the Modern Ocean, Biogeosciences, 18, 1269–1289, https://doi.org/10.5194/bg-18-1269-2021, 2021.

Trenberth, K. E. and Smith, L.: The Mass of the Atmosphere: A Constraint on Global Analyses, Journal of Climate, 18, 864–875,

515 https://doi.org/10.1175/JCLI-3299.1, 2005.

Volk, T. and Hoffert, M. I.: Ocean Carbon Pumps : Analysis of Relative Strengths and Efficiencies in Ocean-Driven Atmospheric CO_2 Changes, in: The Carbon Cycle and Atmospheric CO_2 : Natural Variations Archean to Present, edited by Sundquist, E. T. and Broecker, W. S., vol. 32 of *Geophysical Monograph Series*, pp. 99–110, American Geophysical Union (AGU), Washington (DC), https://doi.org/10.1029/GM032p0099, 1985.

520 Wanninkhof, R.: Relationship between wind speed and gas exchange over the ocean revisited, Limnology and Oceanography: Methods, 12, 351–362, https://doi.org/10.4319/lom.2014.12.351, 2014.

Williams, D. R.: Earth Fact Sheet, https://nssdc.gsfc.nasa.gov/planetary/factsheet/earthfact.html, last access: 31st August 2023, 2023.

Zeebe, R. E. and Wolf-Gladrow, D. A.: CO_2 in Seawater: Equilibrium, Kinetics, Isotopes, vol. 65 of *Elsevier Oceanography Book Series*, Elsevier Science Publishing, Amsterdam, The Netherlands, 2001.